THE ASTROPHYSICAL JOURNAL, 486:847–861, 1997 September 10

LONG-SLIT SPECTROPHOTOMETRY OF THE H II REGIONS GUM 38A AND GUM 38B

LÉO GIRARDI,[1] EDUARDO BICA, AND MIRIANI G. PASTORIZA[2]
Instituto de Física, Universidade Federale do Rio Grande do Sul, Caixa Postal 15051, 91501-970 Porto Alegre RS, Brazil
AND
CLÁUDIA WINGE[1,2]
Space Telescope Science Institute, Baltimore, MD 21218
Received 1993 October 8; accepted 1997 April 14

ABSTRACT

We present new long-slit spectrophotometric observations in the range 3700–7200 Å of the H II regions Gum 38a and Gum 38b (RCW 57). We study the spatial distribution of reddening and excitation throughout the complex by means of emission-line intensities. From the strong reddening difference, we confirm that Gum 38a and Gum 38b are two individual complexes, the former being in the foreground. We derive chemical abundances in both nebulae, the results of which are similar to those of the Orion Nebula. This is consistent with the fact that the three nebulae are located at similar Galactocentric distances. We also discuss the general ionization structure of the complexes based on the spectral properties of several filaments and diffuse emission around the central bright knots of Gum 38a and beyond. In particular, we found an interesting filament with strong [O I] $\lambda\lambda$6300, 6364 lines.

Subject headings: H II regions — ISM: abundances — ISM: individual (RCW 57) — ISM: structure

1. INTRODUCTION

The RCW 57 complex (Rodgers, Campbell, & Whiteoak 1960) consists of several H II regions distributed over an area of $\sim 60' \times 40'$ in Carina (for a global image of the complex, see Block 1990). The western and eastern parts were designated, respectively, 38a and 38b, in Gum's (1955) catalog. The fan-shaped complex Gum 38a contains several bright knots (NGC 3576, 3579, 3581, 3582, 3584, and 3586), which are embedded in a large system of diffuse emission, gas filaments, and dust patches; its morphology resembles that of the Orion Nebula, and it might be a candidate for "champagne flows" at a molecular cloud edge (Tenorio-Tagle 1979). The central part of Gum 38b is NGC 3603, which designates also the rich star cluster embedded therein. An inspection of ESO/SERC Sky Survey *B* plates indicates strong absorption south of both complexes, suggesting the presence of a molecular/dust cloud. Indeed, Goss & Radhakrishnan (1969) showed that Gum 38a and 38b are associated with two different molecular clouds, at different radial velocities. From 21 cm absorption profiles, Goss et al. (1972) determined kinematic distances of 3.6 and 8.4 kpc, respectively, to Gum 38a and 38b. This places both regions at the two intersection points of the Carina arm along the line of sight $\ell = 291°$. Both complexes have been mapped in CO (Goss & Radhakrishnan 1969; Gillespie et al. 1977), neutral hydrogen (Retallack & Goss 1980), radio continuum (Shaver & Goss 1970), and infrared (Kuiper et al. 1987; Ghosh et al. 1989). All these works indicate concentrations of gas and dust at positions coincident with the brighter knots of Gum 38a and Gum 38b (therein referred to as G291.3 − 0.7 and G291.6 − 0.5, respectively).

Concerning Gum 38a, in NGC 3581 and NGC 3582, gas ionization might be attributed to the B0–B0.5 V stars HD 97499 and CPD −60°2641 (Crampton & Georgelin 1975). These two stars, together with HD 97319 (O9.5 Ib) and HD 97484 (O5), are the main components of an OB association (Humphreys 1978; therein designated as NGC 3576 but applying to Gum 38a as a whole) to which a distance modulus $(m - M)_0 = 12.47 \pm 0.28$ (3.1 ± 0.4 kpc) was determined. It is not clear if other isolated bright knots such as NGC 3576 and NGC 3586 have their own ionizing sources or are ionized by photons from the stars in NGC 3581 and 3582. The central brighter knot NGC 3581 hosts a group of five infrared sources (Frogel & Persson 1974) believed to consist of massive young stellar objects embedded in the molecular cloud, including the remarkable source IRS 1 (Moneti 1992).

In the H II complex Gum 38b, the massive star cluster NGC 3603 has a compact unresolved core (HD 97950) known as a similar case to 30 Doradus/NGC 2070/R 136a in the LMC. HD 97950 contains at least 10 massive stars, including two WN and several O stars, and provides the bulk of ionizing photons (Melnick, Tapia, & Terlevich 1989, hereafter MTT89). These authors derived a distance modulus $(m - M)_0 = 14.3$ (7.2 kpc) for the central stars. Several dating methods give an age of ~ 2.5 Myr to the cluster (Santos & Bica 1993).

Gum 38b has been studied by means of imaging in optical and infrared emission lines (Balick, Boeshaar, & Gull 1980; Lacy, Beck, & Geballe 1982). In optical spectroscopy, Shaver et al. (1983) studied a single slit position on NGC 3581, and MTT89 estimated the oxygen abundance from a spectrum of NGC 3603. In the present work, we provide new spectrophotometric observations in several slit positions throughout RCW 57 (§ 2) in order to study the spatial distribution of physical parameters and chemical abundances of the ionized gas (§ 3). They also allow us to probe the chemical abundances along the Carina arm, at Galactocentric distances similar to the Sun's. The concluding remarks of this work are presented in § 4.

2. OBSERVATIONS

The long-slit spectra were obtained during seven nights in 1992 May–July with the Cerro Tololo Inter-American

[1] CNPq fellow.
[2] Visiting Astronomer, Cerro Tololo Inter-American Observatory. CTIO is operated by AURA, Inc., under contract to the National Science Foundation.

Observatory (CTIO) 1 m telescope. The spectrograph plus 2D-FRUTTI detector provided spectra in the range 3700–7200 Å, with a mean resolution of 7 Å (FWHM of emission lines). The slit length corresponds to 5.2 oriented in the east-west direction and the slit width to 5″ on the sky. The mean spatial resolution was of ~5″ (FWHM of stellar profiles). The spectra were reduced at the Instituto de Física (Universidade Federal do Rio Grande do Sul) computer center, with the IRAF package version 2.10, using standard procedures. At least five standard stars per night, from the Stone & Baldwin (1983) list, were used for flux calibrations. The different slit positions are indicated in Figure 1, and the log of observations is presented in Table 1. The lines of sight include knots, diffuse surrounding regions, and filaments.

For each slit position, 600 s sky spectra were taken at positions $\Delta\alpha = 772''$, $\Delta\delta = 219''$ and $\Delta\alpha = 836''$, $\Delta\delta = 1394''$ relative to HD 97452, which are regions of relatively fewer stars to the north and south of RCW 57 (Fig. 1). These sky spectra also contained some faint nebular and stellar emissions, which we assumed were representative of the Galactic foreground/background.

Spectral extractions in each slit were based not only on peaks in the light profiles but also on line ratio profiles that indicated different extinction/excitation conditions. As an example, from slit position 1a we extracted spectra 1a1, 1a2, and 1a3, corresponding to the three peaks observed in the slit centered on NGC 3581 (Fig. 2). The central coordinates and the lengths of each spectral aperture are given in Table 2, and they are indicated as well in Figure 1. Figure 3 shows some representative spectra.

The flux in each emission line was calculated by integration over an interval $\Delta\lambda = 2\text{FWHM} \simeq 14$ Å. The lines $\lambda\lambda$6300, 6312, $\lambda\lambda$6548, 6563, 6583, and $\lambda\lambda$6717, 6731, partially blended, were separated by means of a Gaussian fitting algorithm, which produced rms residuals similar to those of the neighboring continuum. In both methods, the flux measurement involves two continuum placements, and the errors were estimated as $\sigma_{F_\lambda} = 2^{1/2}\Delta\lambda\sigma_{\rm cont}$, with $\sigma_{\rm cont}$ being the rms noise in the continuum next to the line. The rms scatter in sensitivity curves obtained from different calibration stars implies uncertainties of ~2% in fluxes for lines near the red and blue spectral ends.

Table 3 presents the observed line fluxes relative to $F_{H\beta} = 100$ for the different extractions. The quoted errors reflect the uncertainties in the continuum placement. The

TABLE 1

LOG OF THE OBSERVATIONS

Region and Slit Position	Date (1992)	Exposure Time (s)	Comments
Gum 38a:			
1a.....	May 22	1800	NGC 3581: very bright
2a.....	May 22	2400	NGC 3581, 3586: bright
3a.....	May 22	1800	NGC 3579, 3584: very bright
4a.....	May 22	1800	NGC 3579, 3584: bright
5a.....	Jun 3	1800	NGC 3576: bright
6a.....	Jun 3	1800	NGC 3586: bright
7a.....	Jun 3	1800	Star + weak knot
8a.....	Jun 3	1800	Filament E: intermediate
9a.....	Jul 27	1800	Filament N: intermediate
10a	Jul 31	1800	NGC 3579 N extension: bright
11a	Jul 31	1800	Filament NE: bright
Gum 38b:			
1b	May 22	2400	NGC 3603 NE: intermediate
2b	Jun 3	1800	NGC 3603 SE: intermediate
3b	Jul 29	1800	Diffuse emission to NE
4b	Jul 29	1800	Diffuse emission more to NE

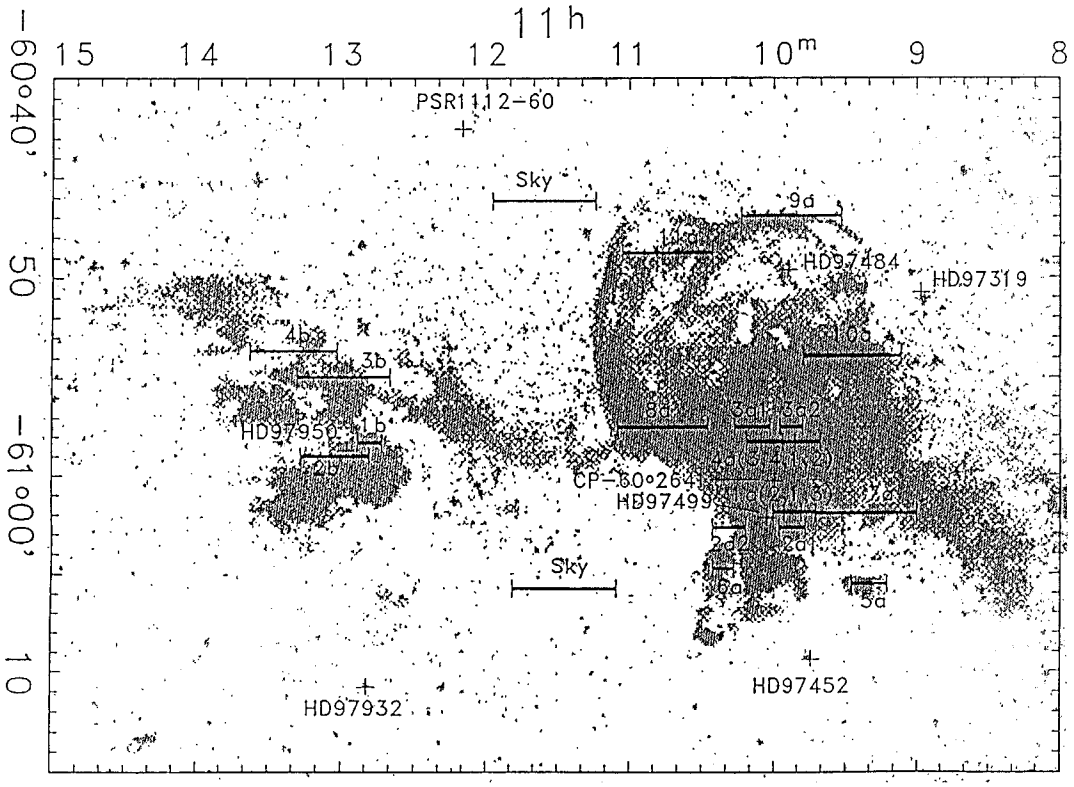

FIG. 1.—Slit positions and apertures for the extracted spectra, superposed on an image of RCW 57 (from the ESO/SERC Sky Survey *R* plate). Assumed distances of 3.1 kpc for Gum 38a and 7.2 kpc for Gum 38b give scales of 0.91 pc arcmin^{-1} and 2.1 pc arcmin^{-1}, respectively.

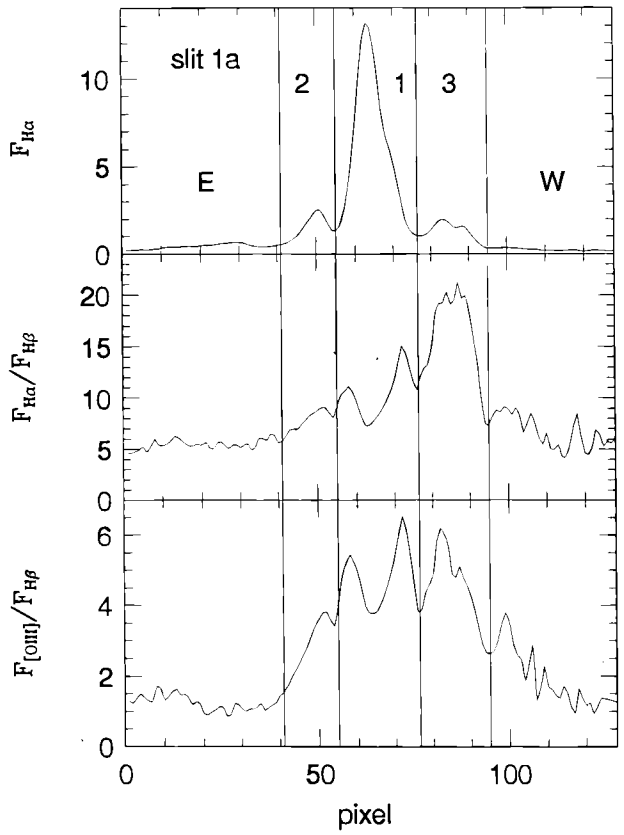

FIG. 2.—Light profiles along the slit position 1a, in Hα, Hα/Hβ, and [O III] λλ4959, 5007/Hβ. The scale is 2".44 pixel^{-1}. Vertical lines encompass the intervals in which spectra 1a1, 1a2, and 1a3 were extracted.

TABLE 2

CENTRAL COORDINATES AND APERTURE LENGTHS FOR INDIVIDUAL EXTRACTED SPECTRA

Region and Slit Position	Δα (arcsec)	Δδ (arcsec)	Length (arcsec)
Gum 38a:			
1a1	56	449	53
1a2	99	449	32
1a3	7	449	45
2a1	57	403	81
2a2	248	403	99
3a1	178	712	108
3a2	60	712	70
4a1	87	666	37
4a2	10	666	76
4a3	173	666	45
4a4	119	666	66
5a.....	−175	232	107
6a.....	265	279	61
7a.....	−166	446	308
8a.....	448	712	272
9a.....	59	1347	303
10a	−124	929	294
11a	434	1239	273
Gum 38b:			
1b	8	749	72
2b	96	707	204
3b	69	950	277
4b	218	1028	262

NOTE.—Δα and Δδ are the offset positions from HD 97452 (SAO 251311, $\alpha_{1950} = 11^h09^m44^s.4$, $\delta_{1950} = -61°09'23".8$) for Gum 38a and from HD 97932 ($\alpha_{1950} = 11^h12^m49^s.7$, $\delta_{1950} = -61°10'46".9$) for Gum 38b.

lower part of this table presents the observed value of $F_{H\beta}$ in ergs^{-1} cm^{-2}.

3. PHYSICAL PARAMETERS

The representative spectra in Figure 3 suggest a range of physical conditions throughout both H II region complexes. The region at slit position 1a1 is more excited and denser than the neighboring one at 1a2 (Fig. 3*a*), as denoted, respectively, by the line ratios [O III] λλ4959, 5007/Hβ and [S II] λ6717/λ6731. The latter ratio also denotes a lower density in the spectra at slit positions 2a1 and 3a1, and the Hα/Hβ ratio indicates a significantly lower extinction for that in 3a1. All these regions are in the brightest parts of Gum 38a. The whole excitation range can be seen in Figure 3*b*, where spectra 5a and 8a (corresponding, respectively, to the knot NGC 3576 and to the eastern filament) present extremely faint [O III] lines, whereas NGC 3579 is very excited. In the filamentary region at slit position 9a (Fig. 3*c*), the [O III] lines are moderately weak, but [O I] λλ6300, 6364 is unusually strong. Figure 3*c* also shows two representative spectra of Gum 38b, which present both larger excitation and larger extinction than those in Gum 38a.

3.1. *Extinction Correction*

Before the line fluxes presented in Table 3 can be used for the analysis of physical conditions, they must be corrected for the interstellar reddening. There are two commonly used ways of applying this correction. We will perform both separately, since they give significantly different results, as will be discussed in § 3.2 below.

3.1.1. *The Savage & Mathis Extinction Curve*

This is the more frequently used extinction correction. We use Osterbrock's (1988) version of Savage & Mathis's (1979) extinction curve, according to

$$\left(\frac{F_\lambda}{F_{H\beta}}\right)_{\rm intr.} = \left(\frac{F_\lambda}{F_{H\beta}}\right)_{\rm obs.} 10^{-c[f(\lambda)-f(H\beta)]}, \quad (1)$$

in which $f(\lambda) - f(H\beta)$ is the mean interstellar extinction curve relative to Hβ and c is a measure of the amount of extinction. We derive c from the ratio between the Balmer recombination lines of hydrogen. These line ratios are slightly dependent on the electron temperature and on the assumptions about the optical depth of the nebula to Lyman photons (including the effects of dust; see Hummer & Storey 1992 for a thorough discussion).

As a first step, we assume case B of recombination theory for the line ratio Hα/Hβ. According to Hummer & Storey's (1987) results, we have $(H\alpha/H\beta)_{\rm intr.} = 2.863(T_e/10^4\ {\rm K})^{-0.066}$; this formula was obtained from a least squares fit to the emissivity values presented by Storey & Hummer (1995) for case B, with $N_e = 100$ cm^{-3}, and at temperatures around $T_e = 10^4$ K. For a few cases (see below), we will assume case A conditions, which, according to Hummer & Storey calculations, is given by $(H\alpha/H\beta)_{\rm intr.} = 2.821(T_e/10^4\ {\rm K})^{-0.093}$. The adopted T_e values are those derived from the central extractions, where the line [O III] λ4363 was available (see Table 4 and § 3.4). Notice, however, that the dependence of the Hα/Hβ ratio on T_e is very weak. Table 4 presents the line fluxes relative to Hβ, obtained according to this procedure, together with the corresponding c values for each spectrum.

We show in Figure 4 the spatial distribution of reddening, taking the $E_{B-V} = 0.7c$ relation derived from the

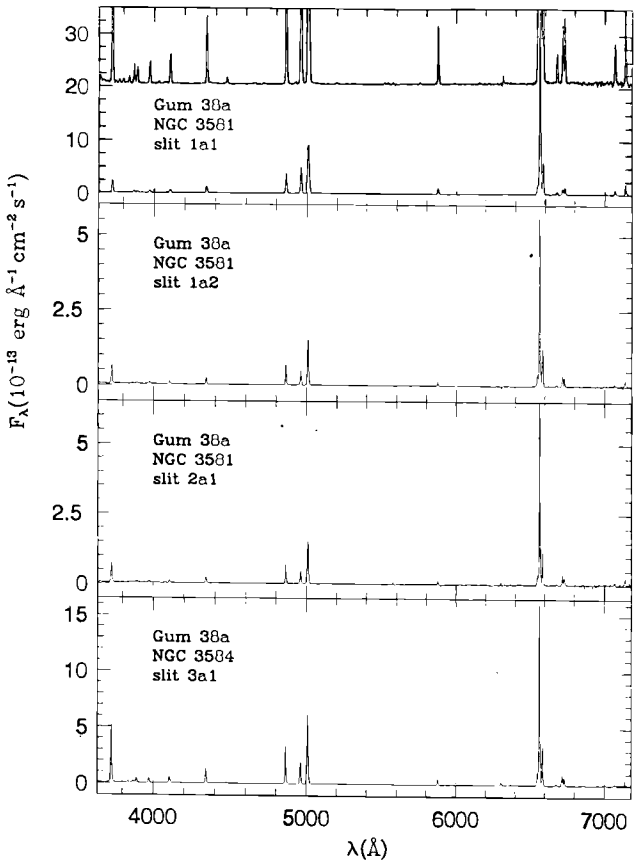

FIG. 3*a*

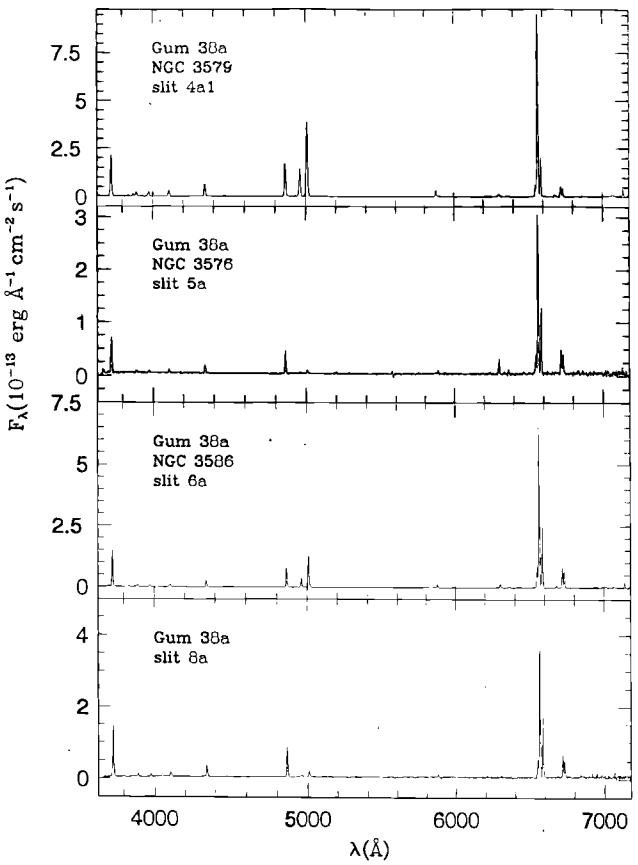

FIG. 3*b*

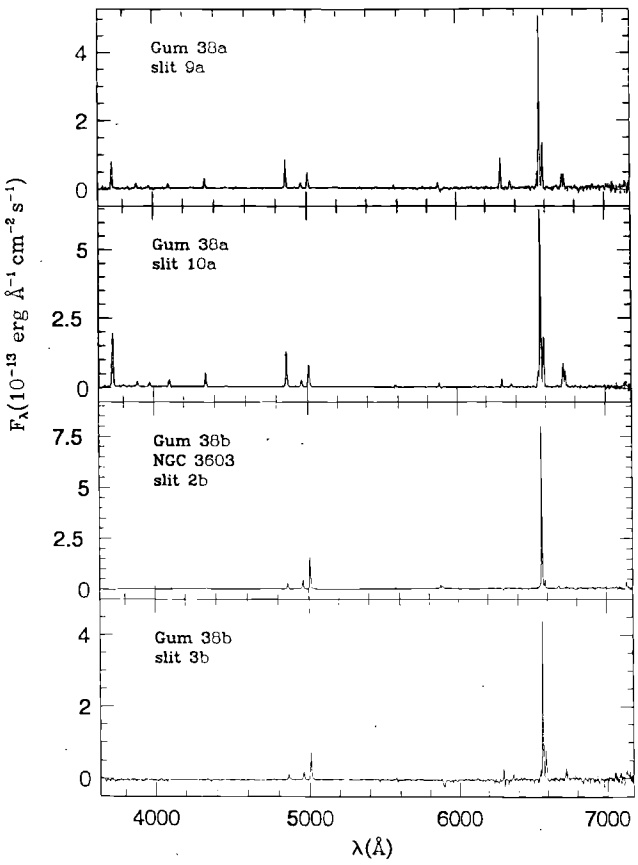

FIG. 3*c*

FIG. 3.—Some representative spectral extractions, namely, (*a*) 1a1, 1a2, 2a1, and 3a1 (extraction 1a1 is 10 times enlarged at the top); (*b*) 4a1, 5a, 6a, and 8a; and (*c*) 9a, 10a, 2b, and 3b. See comments in the text.

TABLE 3

OBSERVED LINE FLUXES RELATIVE TO $F_{H\beta} = 100$

Line	λ	1a1	1a2	1a3	2a1	2a2	3a1	3a2	4a1	4a2	4a3	4a4
[O II]	3727	65.5 ± 0.4	103.5 ± 1.7	87.4 ± 2.6	122.4 ± 4.0	129.3 ± 2.2	175.9 ± 0.5	178.2 ± 1.6	133.3 ± 0.8	182.4 ± 1.0	148.5 ± 1.0	183.0 ± 1.1
H12	3749	1.0 ± 0.4	…	…	…	…	…	…	…	…	2.9 ± 0.9	4.3 ± 1.2
H11, O III	3771	1.8 ± 0.3	…	…	…	…	2.1 ± 0.4	…	1.8 ± 0.8	3.0 ± 0.9	3.3 ± 0.9	1.5 ± 1.2
H10	3798	2.0 ± 0.3	2.3 ± 1.5	…	3.5 ± 3.4	…	3.2 ± 0.4	4.0 ± 1.5	3.4 ± 0.7	2.7 ± 0.9	4.4 ± 0.8	4.5 ± 1.3
He I	3820	…	…	…	…	…	…	…	…	…	…	…
H9	3834	3.3 ± 0.3	1.7 ± 1.4	7.3 ± 2.1	…	…	5.5 ± 0.4	6.5 ± 1.4	4.4 ± 0.7	6.1 ± 0.8	7.1 ± 0.7	9.8 ± 1.3
[Ne III]	3869	9.6 ± 0.3	5.2 ± 1.3	6.4 ± 1.9	8.0 ± 2.8	…	6.7 ± 0.4	4.8 ± 1.3	7.9 ± 0.6	6.8 ± 0.8	8.7 ± 0.7	6.1 ± 1.4
H8, He I	3889	8.4 ± 0.3	7.9 ± 1.3	8.1 ± 1.8	13.0 ± 2.6	6.8 ± 1.5	14.2 ± 0.3	12.9 ± 1.2	13.9 ± 0.6	13.4 ± 0.7	13.9 ± 0.6	17.2 ± 1.4
[Ne III], Hε	3969	11.5 ± 0.2	11.4 ± 1.2	10.9 ± 1.8	14.6 ± 2.0	10.1 ± 1.3	14.7 ± 0.3	14.5 ± 0.9	15.6 ± 0.5	14.4 ± 0.6	15.8 ± 0.5	18.3 ± 1.6
He I	4026	1.0 ± 0.2	…	…	…	…	1.6 ± 0.3	…	…	…	1.5 ± 0.5	4.3 ± 1.3
[S II]	4072	1.1 ± 0.2	1.8 ± 1.0	…	…	…	1.5 ± 0.3	…	…	…	2.0 ± 0.5	3.1 ± 1.3
Hδ, N III	4102	14.3 ± 0.2	15.9 ± 1.0	13.2 ± 1.6	16.0 ± 1.5	17.0 ± 1.0	20.2 ± 0.3	18.5 ± 0.7	18.0 ± 0.4	18.9 ± 0.6	20.8 ± 0.5	19.8 ± 1.1
C II	4627	…	…	…	…	…	…	…	…	…	…	…
Hγ	4340	32.8 ± 0.2	33.2 ± 0.8	29.8 ± 1.3	37.0 ± 0.9	37.7 ± 0.7	40.0 ± 0.2	38.8 ± 0.7	36.7 ± 0.3	39.1 ± 0.5	40.8 ± 0.4	42.0 ± 1.0
[O III]	4363	0.9 ± 0.2	…	…	…	…	0.6 ± 0.3	…	…	…	…	…
He I	4472	3.3 ± 0.1	1.7 ± 0.7	4.0 ± 1.2	3.2 ± 1.0	…	4.4 ± 0.3	3.6 ± 0.5	3.9 ± 0.4	4.0 ± 0.4	3.7 ± 0.4	2.4 ± 1.0
C IV, Fe III	4659	0.5 ± 0.1	…	…	…	…	…	…	…	…	…	…
[Ar IV], He I, [Ne IV]	4713	0.4 ± 0.1	…	…	…	…	0.3 ± 0.2	…	…	…	…	…
Hβ	4861	100.0 ± 0.1	100.0 ± 0.4	100.0 ± 0.9	100.0 ± 0.9	100.0 ± 0.7	100.0 ± 0.2	100.0 ± 0.5	100.0 ± 0.3	100.0 ± 0.4	100.0 ± 0.3	100.0 ± 0.6
He I	4922	1.5 ± 0.1	…	…	…	…	1.3 ± 0.2	2.2 ± 0.5	1.5 ± 0.3	1.7 ± 0.4	1.7 ± 0.3	…
[O III]	4930	…	…	…	…	…	1.3 ± 0.2	…	…	…	…	…
[O III]	4959	128.4 ± 0.1	74.1 ± 0.4	111.7 ± 0.9	69.1 ± 0.9	34.5 ± 0.7	63.4 ± 0.2	47.6 ± 0.5	79.6 ± 0.3	70.9 ± 0.4	64.5 ± 0.3	39.5 ± 0.6
[O III]	5007	310 ± 0.1[a]	243.1 ± 0.5	372.5 ± 0.9	226.2 ± 0.9	115.1 ± 0.7	200.1 ± 0.2	154.1 ± 0.5	243.0 ± 0.3	225.7 ± 0.4	203.6 ± 0.3	126.9 ± 0.6
[N I]	5199	0.9 ± 0.2	…	2.3 ± 1.2	3.5 ± 0.8	5.3 ± 0.7	0.8 ± 0.3	2.0 ± 0.5	0.7 ± 0.3	1.4 ± 0	1.6 ± 0.3	3.0 ± 0.8
[Cl III]	5518	1.0 ± 0.2	…	…	…	…	0.7 ± 0.3	…	…	…	…	…
[Cl III]	5538	0.8 ± 0.2	…	…	…	…	0.4 ± 0.3	…	…	…	…	…
[N II]	5755	1.1 ± 0.2	…	…	…	…	0.7 ± 0.4	…	…	…	0.6 ± 0.4	…
C IV	5806	0.5 ± 0.2	…	…	…	…	…	…	…	…	…	…
He I	5876	27.5 ± 0.2	20.0 ± 1.0	31.2 ± 2.2	9.0 ± 1.7	…	16.0 ± 0.4	37.6 ± 0.9	18.3 ± 0.4	19.8 ± 0.5	14.2 ± 0.5	15.0 ± 1.1
[O I]	6300	…	…	…	…	…	7.2 ± 0.7	10.7 ± 1.1	8.4 ± 0.5	18.3 ± 0.8	10.1 ± 0.7	25.0 ± 1.3
[S III]	6312	4.0 ± 0.3	…	…	…	…	2.1 ± 0.7	…	1.4 ± 0.5	8.9 ± 0.8	…	…
[O I]	6364	…	…	…	…	…	2.8 ± 0.7	4.0 ± 1.2	3.2 ± 0.5	4.3 ± 0.8	2.4 ± 0.7	9.5 ± 1.2
[N II]	6548	49.9 ± 0.4	62.4 ± 1.7	81.4 ± 3.5	54.7 ± 2.7	47.3 ± 2.2	34.4 ± 0.7	42.0 ± 1.8	33.0 ± 0.6	54.6 ± 1.2	27.4 ± 0.8	49.7 ± 1.4
Hα	6563	871.4 ± 0.4	803.6 ± 1.8	1646.0 ± 3.6	848.6 ± 2.7	594.8 ± 2.2	449.7 ± 0.7	426.5 ± 1.9	519.8 ± 0.6	561.3 ± 1.2	429.3 ± 0.8	438.0 ± 1.7
[N II]	6583	151.2 ± 0.4	185.6 ± 1.8	238.5 ± 3.8	154.6 ± 2.7	156.0 ± 2.2	104.1 ± 0.7	121.7 ± 2.0	107.0 ± 0.7	166.3 ± 1.1	83.6 ± 0.8	117.4 ± 1.8
He I	6678	12.0 ± 0.4	7.6 ± 2.0	21.2 ± 4.3	7.6 ± 2.8	…	5.1 ± 0.7	5.6 ± 2.0	7.1 ± 0.8	8.0 ± 1.4	5.3 ± 1.0	7.5 ± 2.1
[S II]	6717	25.1 ± 0.4	48.3 ± 2.1	44.2 ± 4.4	49.3 ± 2.8	49.2 ± 2.5	28.4 ± 0.7	48.6 ± 1.9	27.7 ± 0.8	49.4 ± 1.4	26.9 ± 1.1	45.5 ± 2.1
[S II]	6731	29.1 ± 0.4	44.4 ± 2.2	52.8 ± 4.5	37.9 ± 2.8	42.5 ± 2.6	22.4 ± 0.7	34.6 ± 1.8	23.8 ± 0.8	41.8 ± 1.4	21.0 ± 1.1	38.6 ± 2.1
He I	7065	17.1 ± 0.9	10.0 ± 4.6	30.7 ± 8.8	7.1 ± 6.2	…	3.8 ± 1.7	…	…	4.2 ± 1.8	2.2 ± 2.2	…
[Ar III]	7136	46.3 ± 0.9	30.3 ± 4.6	110.3 ± 8.8	43.6 ± 6.2	19.4 ± 2.6	11.6 ± 1.7	9.8 ± 3.4	17.2 ± 1.3	17.5 ± 1.8	8.9 ± 2.2	16.2 ± 3.6
$F_{H\beta,obs.}$ (10^{-12} ergs s^{-1} cm^{-2})		3.45	0.59	0.34	0.59	0.79	2.78	1.18	1.51	1.74	1.51	0.83

TABLE 3—*Continued*

Line	λ	5a	6a	7a	8a	9a	10a	11a	1b	2b	3b	4b
[O II]	3727	162.1 ± 5.1	179.2 ± 2.1	162.3 ± 3.0	181.7 ± 2.4	108.0 ± 4.8	169.0 ± 2.0	139.2 ± 4.7	...	...	...	...
H12	3749	...	...	...	...	...	...	...	...	...	...	...
H11, O III	3771	...	...	...	2.1 ± 2.1	...	2.4 ± 1.8	...	...	...	...	...
H10	3798	...	1.8 ± 1.8	...	4.5 ± 2.0	...	3.3 ± 1.7	...	...	...	...	...
He I	3820	...	...	...	...	...	...	...	...	...	...	...
H9	3834	...	7.0 ± 1.6	...	2.9 ± 1.7	6.9 ± 4.1	4.9 ± 1.5	...	...	...	...	...
[Ne III]	3869	...	5.2 ± 1.4	...	...	...	3.6 ± 1.3	...	...	...	...	...
H8, He I	3889	9.6 ± 3.2	11.2 ± 1.3	13.4 ± 2.3	13.7 ± 1.4	18.2 ± 3.8	13.7 ± 1.2	18.6 ± 3.2	...	...	...	...
[Ne III], Hε	3969	9.8 ± 1.8	13.2 ± 1.1	12.2 ± 2.3	12.1 ± 1.0	9.6 ± 3.7	12.8 ± 0.9	16.3 ± 2.3	...	...	...	...
He I	4026	...	...	...	...	...	...	...	...	...	...	...
[S II]	4072	...	2.2 ± 0.9	...	...	...	1.2 ± 0.8	...	...	...	...	...
Hδ, N III	4102	13.2 ± 1.8	17.3 ± 0.8	21.7 ± 2.2	18.7 ± 0.9	17.0 ± 2.2	19.6 ± 0.8	21.3 ± 2.0	...	...	...	...
C II	4267	...	...	...	...	...	...	...	...	...	...	...
Hγ	4340	37.6 ± 1.5	36.0 ± 0.8	39.8 ± 1.1	40.5 ± 0.7	36.5 ± 1.6	41.9 ± 0.7	46.5 ± 1.4	...	21.5 ± 1.4	...	...
[O III]	4363	...	...	...	...	...	1.6 ± 0.7	...	...	...	...	...
He I	4472	...	4.3 ± 0.7	3.2 ± 1.3	2.9 ± 0.7	3.2 ± 1.7	2.9 ± 0.6	3.1 ± 1.6	...	...	...	...
C IV, Fe III	4659	...	...	...	...	...	...	...	...	...	...	...
[Ar IV], He I, [Ne IV]	4713	...	...	...	...	...	...	...	...	...	...	...
Hβ	4861	100.0 ± 1.8	100.0 ± 0.7	100.3 ± 1.3	100.0 ± 0.5	100.0 ± 1.0	100 ± 0.4	100.0 ± 1.4	100.0 ± 4.0	100.0 ± 1.7	100.0 ± 5.6	100.0 ± 24.3
He I	4922	...	2.2 ± 0.7	...	...	...	1.2 ± 0.5	...	...	...	18.0 ± 3.9	...
[O III]	4930	...	...	...	...	...	...	...	...	...	...	...
[O III]	4959	5.5 ± 1.7	47.5 ± 0.7	17.5 ± 1.3	8.6 ± 0.5	22.0 ± 1.0	19.0 ± 0.5	31.8 ± 1.5	154.0 ± 4.1	170.3 ± 1.7	145.1 ± 6.2	506.4 ± 64.2
[O III]	5007	17.3 ± 1.6	158.0 ± 0.7	56.5 ± 1.3	28.9 ± 0.6	61.5 ± 1.0	62.3 ± 0.5	100.7 ± 1.2	483.6 ± 4.1	585.9 ± 1.7	469.7 ± 6.4	1930.0 ± 65.6
[N I]	5199	5.1 ± 1.6	2.2 ± 0.8	...	...	...	2.3 ± 0.5	...	...	...	...	...
[Cl III]	5518	...	...	...	...	...	...	...	...	...	...	...
[Cl III]	5538	...	...	...	...	...	...	...	...	...	...	...
[N II]	5755	...	...	...	...	...	...	...	...	...	...	...
C IV	5806	...	...	...	...	...	...	...	...	...	...	...
He I	5876	...	15.8 ± 1.1	...	6.9 ± 1.1	4.5 ± 1.2	4.2 ± 0.9	21.8 ± 2.6	14.6 ± 5.0	96.6 ± 2.9	...	...
[O I]	6300	51.3 ± 4.3	19.1 ± 1.3	12.7 ± 3.5	8.9 ± 1.6	87.1 ± 4.0	19.4 ± 1.5	...	...	...	72.4 ± 26.4	4234.3 ± 260.1
[S III]	6312	...	3.4 ± 1.3	...	...	...	...	...	...	...	...	...
[O I]	6364	14.4 ± 4.4	5.3 ± 1.3	5.4 ± 3.2	...	25.8 ± 4.1	7.7 ± 1.5	...	...	...	83.1 ± 24.3	1141.4 ± 262.9
[N II]	6548	83.8 ± 5.1	99.0 ± 1.7	41.2 ± 3.7	50.9 ± 1.5	51.0 ± 3.9	49.6 ± 1.5	33.9 ± 3.9	32.7 ± 6.5	47.8 ± 5.2	148.1 ± 25.7	1169.3 ± 233.0
Hα	6563	647.8 ± 5.2	724.6 ± 1.7	463.4 ± 3.8	460.6 ± 1.5	583.5 ± 3.8	480.2 ± 1.5	497.9 ± 3.8	2158.3 ± 6.5	2613.3 ± 5.3	2827.6 ± 26.3	16700.0 ± 227.9
[N II]	6583	275.4 ± 5.3	296.2 ± 1.8	133.8 ± 4.0	163.9 ± 1.6	149.9 ± 3.7	146.8 ± 1.5	107.5 ± 3.6	95.6 ± 6.5	121.1 ± 5.5	456.5 ± 27.2	4265.7 ± 221.1
He I	6678	...	10.5 ± 1.9	...	5.0 ± 1.7	12.7 ± 4.2	6.1 ± 1.6	...	39.2 ± 7.6	43.8 ± 6.7	...	...
[S II]	6717	95.5 ± 5.3	79.6 ± 2.0	38.2 ± 4.9	62.9 ± 1.7	56.2 ± 4.9	67.1 ± 1.7	40.7 ± 4.2	22.9 ± 8.5	19.7 ± 7.4	134.1 ± 25.7	1730.7 ± 240.6
[S II]	6731	76.1 ± 5.2	79.9 ± 2.0	28.9 ± 4.9	49.5 ± 1.7	46.6 ± 5.3	48.7 ± 1.7	26.6 ± 4.4	12.9 ± 8.9	29.9 ± 7.8	118.6 ± 25.1	1462.9 ± 246.3
He I	7065	...	...	...	...	...	...	...	22.3 ± 12.8	25.6 ± 11.4	...	...
[Ar III]	7136	...	27.1 ± 4.1	...	...	...	...	37.7 ± 8.0	...	122.7 ± 11.4	186.4 ± 33.9	917.1 ± 357.1
$F_{H\beta,obs.}$ (10^{-12} ergs s^{-1} cm^{-2})		0.36	0.73	0.78	1.57	0.67	2.1	0.63	0.42	0.45	0.15	0.04

[a] Saturated line.

TABLE 4

DERIVED LINE FLUXES RELATIVE TO Hβ

Line	λ	1a1	1a2	1a3	2a1	2a2	3a1	3a2	4a1	4a2	4a3	4a4
[O II]	3727	151.4 ± 0.9	224.8 ± 3.7	326.4 ± 9.8	276.9 ± 9.1	223.7 ± 3.8	245.4 ± 0.6	239.6 ± 2.2	208.2 ± 1.3	301.9 ± 1.6	200.7 ± 1.3	251.1 ± 1.6
H12	3749	2.3 ± 0.8	...	...	...	...	...	...	...	...	3.9 ± 1.2	5.8 ± 1.6
H11, O III	3771	4.0 ± 0.8	...	...	...	...	2.9 ± 0.6	...	2.8 ± 1.2	4.9 ± 1.4	4.4 ± 1.2	2.0 ± 1.6
H10	3798	4.4 ± 0.7	4.8 ± 3.1	...	7.4 ± 7.3	...	4.3 ± 0.6	5.3 ± 1.9	5.1 ± 1.1	4.2 ± 1.4	5.8 ± 1.1	6.1 ± 1.7
He I	3820	...	...	...	...	...	...	...	...	...	...	...
H9	3834	7.1 ± 0.6	3.3 ± 2.9	23.9 ± 6.9	...	...	7.5 ± 0.5	8.5 ± 1.8	6.5 ± 1	9.6 ± 1.3	9.3 ± 1	13.0 ± 1.8
[Ne III]	3869	19.9 ± 0.6	10.2 ± 2.6	20.0 ± 6.1	16.2 ± 5.6	...	8.9 ± 0.5	6.2 ± 1.6	11.6 ± 0.9	10.5 ± 1.2	11.3 ± 0.9	8.0 ± 1.8
H8, He I	3889	17.1 ± 0.5	15.3 ± 2.5	24.8 ± 5.6	26.0 ± 5.2	10.9 ± 2.4	18.8 ± 0.5	16.6 ± 1.6	20.2 ± 0.9	20.6 ± 1.1	17.9 ± 0.8	22.5 ± 1.9
[Ne III], Hϵ	3969	22.1 ± 0.4	20.8 ± 2.1	30.4 ± 4.9	27.6 ± 3.8	15.5 ± 2.0	19.0 ± 0.4	18.2 ± 1.2	22.0 ± 0.7	212 ± 0.8	20.0 ± 0.6	23.4 ± 2.0
He I	4026	1.9 ± 0.3	...	...	...	...	2.1 ± 0.4	...	...	...	1.9 ± 0.6	5.5 ± 1.7
[S II]	4072	2.0 ± 0.3	3.0 ± 1.8	...	...	...	1.9 ± 0.4	...	...	...	2.5 ± 0.6	3.9 ± 1.6
Hδ, N III	4102	25.2 ± 0.3	26.8 ± 1.7	32.3 ± 4.0	27.9 ± 2.6	24.7 ± 1.5	25.3 ± 0.4	22.6 ± 0.9	24.3 ± 0.6	26.7 ± 0.9	25.5 ± 0.6	24.5 ± 1.4
C II	4267	...	...	...	...	...	...	...	...	...	...	...
Hγ	4340	48.4 ± 0.2	47.5 ± 1.1	54.9 ± 2.4	54.1 ± 1.4	48.6 ± 0.9	46.7 ± 0.3	44.6 ± 0.8	45.1 ± 0.4	49.4 ± 0.6	46.9 ± 0.4	48.6 ± 1.1
[O III]	4363	1.4 ± 0.2	...	...	...	...	0.7 ± 0.3	...	...	...	...	...
He I	4472	4.4 ± 0.2	2.2 ± 0.9	6.5 ± 1.9	4.3 ± 1.3	...	5.0 ± 0.3	4.0 ± 0.6	4.6 ± 0.4	4.8 ± 0.5	4.1 ± 0.5	2.7 ± 1.1
C IV, [Fe III]	4659	0.6 ± 0.2	...	...	...	...	...	...	...	...	...	...
[Ar IV], He I, [Ne IV]	4713	0.5 ± 0.2	...	...	...	...	0.3 ± 0.2	...	...	...	...	...
Hβ	4861	100.0 ± 0.1	100.0 ± 0.4	100.1 ± 0.9	100.0 ± 0.9	100.0 ± 0.7	100.0 ± 0.2	100.0 ± 0.5	100.0 ± 0.3	100.0 ± 0.4	100.0 ± 0.3	100.0 ± 0.6
He I	4922	1.4 ± 0.1	...	...	...	...	1.3 ± 0.2	2.2 ± 0.5	1.5 ± 0.3	1.6 ± 0.4	1.6 ± 0.3	...
[O III]	4930	...	...	...	...	...	1.3 ± 0.2	...	...	...	...	...
[O III]	4959	117.1 ± 0.1	68.0 ± 0.4	96.7 ± 0.8	63.2 ± 0.8	32.5 ± 0.7	61.2 ± 0.2	46.1 ± 0.5	75.8 ± 0.3	67.1 ± 0.4	62.4 ± 0.3	38.1 ± 0.6
[O III]	5007	270.6 ± 0.1[a]	214.3 ± 0.4	300.8 ± 0.8	198.2 ± 0.8	105.4 ± 0.6	189.5 ± 0.2	146.9 ± 0.5	226.1 ± 0.3	208.0 ± 0.4	193.9 ± 0.3[a]	120.5 ± 0.6
[N I]	5199	0.6 ± 0.1	...	1.5 ± 0.7	2.6 ± 0.6	4.4 ± 0.6	0.7 ± 0.2	1.8 ± 0.5	0.6 ± 0.2	1.2 ± 0.3	1.4 ± 0.3	2.6 ± 0.7
[Cl III]	5518	0.6 ± 0.1	...	...	...	...	0.6 ± 0.2	...	...	...	...	...
[Cl III]	5538	0.5 ± 0.1	...	...	...	...	0.3 ± 0.2	...	...	...	...	...
[N II]	5755	0.5 ± 0.1	...	...	...	...	0.5 ± 0.3	...	...	...	0.5 ± 0.3	...
C IV	5806	0.3 ± 0.1	...	...	...	...	...	...	...	...	...	...
He I	5876	12.8 ± 0.1	9.8 ± 0.5	9.3 ± 0.7	4.3 ± 0.8	...	11.8 ± 0.3	28.7 ± 0.7	12.2 ± 0.3	12.5 ± 0.3	10.8 ± 0.4	11.2 ± 0.8
[O I]	6300	...	...	...	...	...	4.9 ± 0.5	7.6 ± 0.8	4.9 ± 0.3	10.1 ± 0.4	7.1 ± 0.5	17.2 ± 0.9
[S III]	6312	1.5 ± 0.1	...	...	...	...	1.4 ± 0.5	...	0.8 ± 0.3	4.9 ± 0.4	...	...
[O I]	6364	...	...	...	...	...	1.9 ± 0.5	2.8 ± 0.8	1.9 ± 0.3	2.3 ± 0.4	1.7 ± 0.5	6.5 ± 0.8
[N II]	6548	16.6 ± 0.1	22.5 ± 0.6	14.4 ± 0.6	18.7 ± 0.9	23.0 ± 1.1	22.2 ± 0.4	28.4 ± 1.2	18.4 ± 0.3	28.1 ± 0.6	18.4 ± 0.5	32.8 ± 0.9
Hα	6563	287.9 ± 0.1	288.3 ± 0.6	288.3 ± 0.6	288.3 ± 0.9	288.3 ± 1.1	289.5 ± 0.4	288.3 ± 1.3	288.3 ± 0.4	288.3 ± 0.6	288.3 ± 0.5	288.3 ± 1.1
[N II]	6583	49.6 ± 0.1	66.1 ± 0.6	41.3 ± 0.7	52.1 ± 0.9	75.3 ± 1.1	66.8 ± 0.4	82.1 ± 1.4	59.1 ± 0.4	85.0 ± 0.5	56.0 ± 0.5	77.1 ± 1.2
He I	6678	3.8 ± 0.1	2.6 ± 0.7	3.5 ± 0.7	2.5 ± 0.9	...	3.2 ± 0.4	3.7 ± 1.4	3.9 ± 0.4	4.0 ± 0.7	3.5 ± 0.7	4.9 ± 1.3
[S II]	6717	7.9 ± 0.1	16.4 ± 0.7	7.1 ± 0.7	15.9 ± 0.9	23.0 ± 1.2	17.9 ± 0.4	32.2 ± 1.2	14.9 ± 0.4	24.6 ± 0.7	17.7 ± 0.7	29.3 ± 1.3
[S II]	6731	9.1 ± 0.1	15.1 ± 0.7	8.4 ± 0.7	12.1 ± 0.9	19.8 ± 1.2	14.0 ± 0.4	22.9 ± 1.2	12.8 ± 0.4	20.7 ± 0.7	13.8 ± 0.7	24.8 ± 1.3
He I	7065	4.7 ± 0.3	3.0 ± 1.4	4.0 ± 1.2	2.0 ± 1.8	...	2.3 ± 1	...	...	2.0 ± 0.8	1.4 ± 1.4	...
[Ar III]	7136	12.3 ± 0.3	8.9 ± 1.3	13.7 ± 1.1	12.0 ± 1.7	8.1 ± 1.1	6.9 ± 1	6.1 ± 2.1	8.5 ± 0.7	7.9 ± 0.8	5.5 ± 1.4	9.8 ± 2.2
$F_{H\beta,intr.}$ (10^{-10} ergs s^{-1} cm^{-2})		3.50	0.41	6.16	0.52	0.14	0.14	0.05	0.15	0.24	0.06	0.04
c		1.30	1.20	2.04	1.26	0.85	0.51	0.46	0.69	0.78	0.46	0.49
$T_{[O II]}$(K)		8770 ± 430	...	...	...	...	8620 ± 980	...	...	...	...	...
$T_{[N II]}$(K)		8380 ± 540	...	...	...	...	7650 ± 1230	...	...	...	8120^{+1550}_{-2010}	...
N_e (cm^{-3})		920 ± 80	400 ± 130	1040 ± 550	<290	290 ± 140	150 ± 50	<150	270 ± 80	240 ± 70	140 ± 90	250 ± 120

TABLE 4—*Continued*

Line	λ	5a	6a	7a	8a	9a	10a	11a	1b	2b	3b	4b
[O II]	3727	299.0 ± 9.4	360.0 ± 4.2	232.4 ± 4.2	259.0 ± 3.4	184.1 ± 8.3	258.9 ± 3.1	210.5 ± 7.1	...	...	...	...
H12	3749	...	...	...	...	...	...	...	...	...	...	...
H11, O III	3771	...	...	...	3.0 ± 3.0	...	3.6 ± 2.7	...	...	...	...	...
H10	3798	...	3.4 ± 3.4	...	6.3 ± 2.7	...	4.9 ± 2.5	...	...	...	...	...
He I	3820	...	...	...	...	...	...	...	...	...	...	...
H9	3834	...	13.0 ± 3.0	...	4.0 ± 2.4	11.1 ± 6.7	7.2 ± 2.1	...	...	...	...	...
[Ne III]	3869	...	9.5 ± 2.6	...	...	...	5.3 ± 1.9	...	...	...	...	...
H8, He I	3889	16.1 ± 5.4	20.2 ± 2.4	18.1 ± 3.2	18.6 ± 1.9	28.6 ± 5.9	19.7 ± 1.8	26.5 ± 4.5	...	...	...	...
[Ne III], Hε	3969	15.8 ± 2.9	22.6 ± 1.8	16.1 ± 3.0	15.9 ± 1.3	14.5 ± 5.6	17.9 ± 1.3	22.5 ± 3.2	...	...	...	...
He I	4026	...	...	...	...	...	...	...	...	...	...	...
[S II]	4072	...	3.5 ± 1.4	...	...	...	1.7 ± 1.1	...	...	...	...	...
Hδ, N III	4102	20.0 ± 2.8	27.7 ± 1.3	27.7 ± 2.9	23.8 ± 1.1	24.4 ± 3.2	26.2 ± 1.1	28.1 ± 2.7	...	...	...	...
C II	4267	...	...	...	...	...	...	...	...	...	...	...
Hγ	4340	50.0 ± 2.0	49.8 ± 1.1	47.0 ± 1.3	47.8 ± 0.8	46.7 ± 2.0	51.0 ± 0.8	56.3 ± 1.8	...	46.8 ± 3.1	...	...
[O III]	4363	...	...	...	...	...	2.0 ± 0.8	...	...	...	...	...
He I	4472	...	5.5 ± 0.9	3.7 ± 1.4	3.3 ± 0.8	3.9 ± 2.0	3.4 ± 0.6	3.6 ± 1.9	...	...	...	...
C IV, [Fe III]	4659	...	...	...	...	...	...	...	...	...	...	...
[Ar IV], He I, [Ne IV]	4713	...	...	...	...	...	...	...	...	...	...	...
Hβ	4861	100.0 ± 1.8	100.0 ± 0.7	100.0 ± 1.3	100.0 ± 0.5	100.0 ± 1.0	100.0 ± 0.4	100.0 ± 1.4	100.0 ± 4.0	100.0 ± 1.7	100.0 ± 5.6	100.0 ± 24.3
He I	4922	...	2.1 ± 0.7	...	...	...	1.2 ± 0.4	...	...	...	16.0 ± 3.5	...
[O III]	4930	...	...	...	...	...	...	...	...	...	...	...
[O III]	4959	5.2 ± 1.6	44.0 ± 0.6	16.9 ± 1.2	8.2 ± 0.5	20.8 ± 1	18.1 ± 0.4	30.4 ± 1.5	130.3 ± 3.5	141.8 ± 1.4	120.0 ± 5.1	361.4 ± 45.8
[O III]	5007	15.6 ± 1.4	141.1 ± 0.6	53.3 ± 1.2	27.3 ± 0.5	56.4 ± 0.9	58.1 ± 0.4	94.2 ± 1.2	377.5 ± 3.2	446.7 ± 1.3	354.7 ± 4.8	1172.1 ± 39.8
[N I]	5199	4.1 ± 1.3	1.7 ± 0.6	...	...	...	2.0 ± 0.4	...	...	...	...	...
[Cl III]	5518	...	...	...	...	...	...	...	...	...	...	...
[Cl III]	5538	...	...	...	...	...	...	...	...	...	...	...
[N II]	5755	...	...	...	...	...	...	...	...	...	...	...
C IV	5806	...	...	...	...	...	...	...	...	...	...	...
He I	5876	...	8.3 ± 0.6	...	5.0 ± 0.8	2.8 ± 0.7	2.9 ± 0.6	14.9 ± 1.8	3.6 ± 1.2	21.0 ± 0.6	...	...
[O I]	6300	25.0 ± 2.1	8.4 ± 0.6	8.3 ± 2.3	5.9 ± 1.1	46.5 ± 2.1	11.7 ± 0.9	...	...	...	9.5 ± 3.4	113.8 ± 7.0
[S III]	6312	...	1.5 ± 0.6	...	...	...	...	...	...	...	...	...
[O I]	6364	6.9 ± 2.1	2.3 ± 0.6	3.5 ± 2.1	...	13.5 ± 2.2	4.6 ± 0.9	...	...	...	10.2 ± 3.0	27.4 ± 6.3
[N II]	6548	37.5 ± 2.3	39.6 ± 0.7	25.7 ± 2.3	32.0 ± 0.9	25.3 ± 1.9	28.3 ± 0.9	19.7 ± 2.3	4.4 ± 0.9	5.3 ± 0.6	15.2 ± 2.6	20.6 ± 4.1
Hα	6563	288.3 ± 2.3	288.3 ± 0.7	288.3 ± 2.4	288.3 ± 0.9	288.3 ± 1.9	273.2 ± 0.9	288.3 ± 2.2	286.7 ± 0.9	286.7 ± 0.6	286.7 ± 2.7	286.7 ± 3.9
[N II]	6583	121.9 ± 2.3	117.1 ± 0.7	82.9 ± 2.5	102.3 ± 1	73.7 ± 1.8	83.2 ± 0.9	62.0 ± 2.1	12.5 ± 0.9	13.1 ± 0.6	45.6 ± 2.7	71.3 ± 3.7
He I	6678	...	4.0 ± 0.7	...	3.1 ± 1.0	6.1 ± 2.0	3.4 ± 0.9	...	4.8 ± 0.9	4.4 ± 0.7	...	...
[S II]	6717	40.8 ± 2.2	30.2 ± 0.8	23.2 ± 3.0	38.5 ± 1.0	26.8 ± 2.3	37.1 ± 0.9	22.9 ± 2.4	2.7 ± 1.0	1.9 ± 0.7	12.1 ± 2.3	24.2 ± 3.4
[S II]	6731	32.4 ± 2.2	30.2 ± 0.8	17.5 ± 3.0	30.2 ± 1.0	22.1 ± 2.5	26.9 ± 0.9	14.9 ± 2.5	1.5 ± 1.1	2.9 ± 0.8	10.6 ± 2.2	20.1 ± 3.4
He I	7065	...	...	...	...	...	...	...	2.1 ± 1.2	1.9 ± 0.9	...	...
[Ar III]	7136	...	9.0 ± 1.4	...	...	...	...	19.6 ± 4.2	...	8.7 ± 0.8	12.1 ± 2.2	7.1 ± 2.8
$F_{H\beta,intr.}$ (10^{-10} ergs s^{-1} cm^{-2})		0.09	0.32	0.04	0.09	0.11	0.17	0.05	6.90	17.8	8.30	...
c		0.95	1.08	0.55	0.55	0.82	0.65	0.64	2.37	2.59	2.68	3.68
$T_{[O III]}$ (K)		...	...	...	...	...	20600^{+5900}_{-5300}	...	9800[b]	...	...	...
$T_{[N II]}$ (K)		...	...	...	...	...	...	...	...	...	...	...
N_e (cm^{-3})		<300	540 ± 90	<490	150 ± 60	220^{+270}_{-200}	<140	<190	<1090	...	<1180	<730

[a] Saturated line. We used 2.96 × [O III] λ4959 throughout the text.
[b] From Melnick et al. 1989.

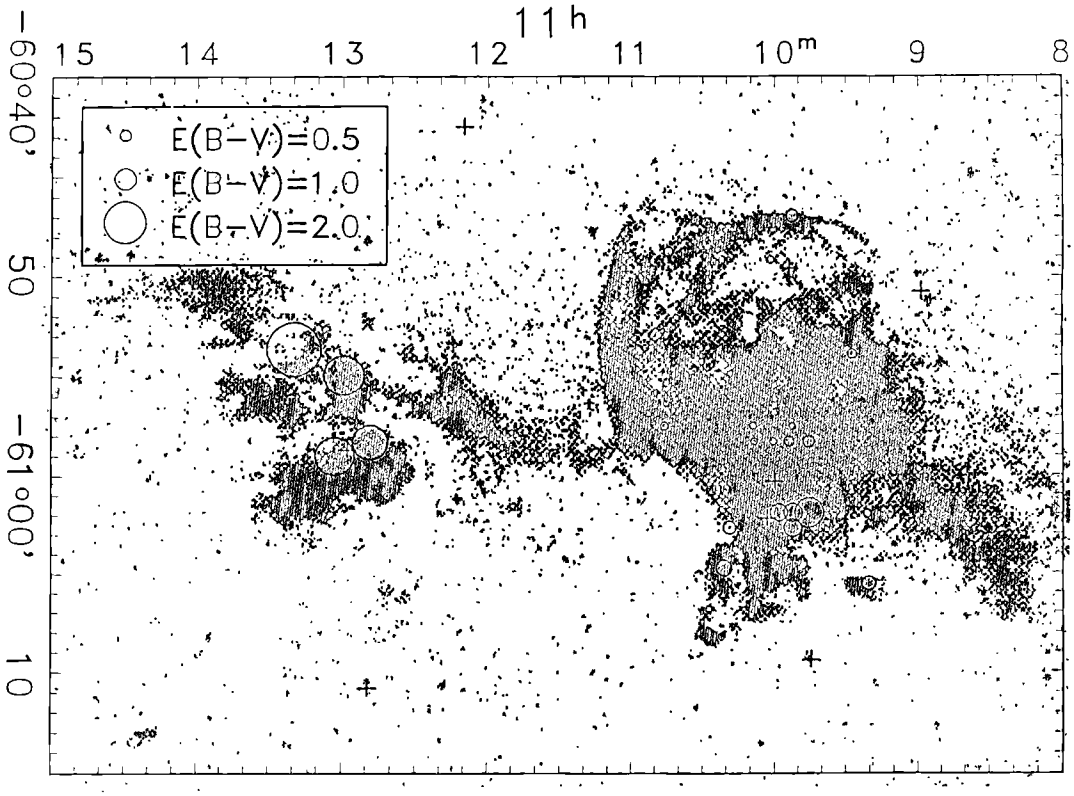

FIG. 4.—Same as Fig. 1, but showing the spatial distribution of E_{B-V}

Savage & Mathis extinction curve. The lowest values in Gum 38a are $E_{B-V} \simeq 0.35$, occurring in the northern parts, which are mostly diffuse and filamentary. This also provides an upper limit for the foreground reddening. This value agrees with $E_{B-V} = 0.32$ for HD 97499, which is the less reddened star of the NGC 3576 OB association (Humphreys 1978). The reddening in Gum 38a increases southward to values of $E_{B-V} \simeq 0.70$ in the bright southern knots, located close to the edge or within the molecular cloud (§ 1). The difference of reddening values within Gum 38a suggest an internal reddening of $\Delta E_{B-V_i} \simeq 0.35$. For Gum 38b, reddening values are considerably higher than those in Gum 38a (Fig. 4), confirming that we are indeed dealing with two different complexes at different distances (§ 1). The lowest value in Gum 38b ($E_{B-V} \simeq 1.65$) suggests that there is a difference of $E_{B-V} = 1.30$ between Gum 38a and Gum 38b, indicating that the mean E_{B-V} gradient over the region internal to the Carina arm is ~ 0.32 kpc^{-1}.

3.1.2. *The Cardelli, Clayton, & Mathis Extinction Curve*

The second method applied in this paper is the generic interstellar extinction curve of Cardelli, Clayton, & Mathis (1989). They derived an analytical formula that gives the extinction curve for different interstellar environments, having as the only parameter the ratio between the total and the selective extinction $R_V = A_V/E_{B-V}$. This ratio is known to vary with the line of sight. The mean extinction curve by Savage & Mathis (1979) is characterized by $R_V = 3.1$, while for stars in dense interstellar environments it is characterized by larger values, as, e.g., that of $R_V = 5.5$ obtained for the stars in the Trapezium in the Orion Nebula (Mathis & Wallenhorst 1981). Thus, Cardelli et al.'s curve describes both cases. The formulae provide absolute values of extinction relative to that in V, i.e., A_λ/A_V. As we have the relationship

$$F_{\lambda,\text{obs.}} = F_{\lambda,\text{intr.}}\, 10^{-0.4 A_\lambda} \tag{2}$$

between observed and intrinsic fluxes in a given spectral line at λ, we can derive the following quantity:

$$(A_{\text{H}\alpha} - A_{\text{H}\beta}) = 2.5 \log \left[\frac{(\text{H}\alpha/\text{H}\beta)_{\text{intr.}}}{(\text{H}\alpha/\text{H}\beta)_{\text{obs.}}}\right], \tag{3}$$

which can then be used for the derivation of the total extinction A_V by means of the A_λ/A_V curve of Cardelli et al.:

$$A_V = \frac{(A_{\text{H}\alpha} - A_{\text{H}\beta})}{A_{\text{H}\alpha}/A_V - A_{\text{H}\beta}/A_V}. \tag{4}$$

With this value of A_V and the A_λ/A_V extinction curve, we then derive the A_λ values necessary to correct the line fluxes of all observed lines by means of equation (2).

Since the complexes Gum 38a and 38b are located at a significant distance from the Sun, much of the observed extinction originates from the diffuse interstellar medium, where $R_V = 3.1$. The remaining extinction should arise in the interior of the H II regions, where an extinction curve with $R_V = 5.5$ is probably more suitable. Therefore, the following procedure is adopted: first, we correct the line fluxes by the foreground reddening, applying the Cardelli et al. (1989) extinction curve with $R_V = 3.1$. The foreground reddening is assumed to be constant for each one of the complexes and equal to $E_{B-V_f} = 0.35$ for Gum 38a and $E_{B-V_f} = 1.5$ for Gum 38b (according to the above subsection). Second, we correct the line fluxes—with the amount necessary to reproduce the theoretical value of Hα/Hβ—using the extinction curve with $R_V = 5.5$.

3.2. *Balmer Line Ratios*

For the spectra of the central regions of Gum 38a, several Balmer lines are available and are measured with a relatively small uncertainty. These can be useful to check the reliability of the extinction corrections applied and/or the suitability of having assumed case B of recombination theory. We stress that in case B Lyman photons are continuously scattered inside the nebula, giving the possibility of photons being continuously lost by means of other cascading channels, eventually resulting in more Balmer lines from the lowest energy levels of hydrogen. On the other hand, under case A conditions, the nebula is transparent to Lyman photons, which leads to different Balmer line ratios. The results of the Storey & Hummer (1995) computations, for pure case A and case B conditions, are recalled in the first columns of Table 5. We notice that the differences between the two cases are not dramatic but could be detected if high-quality spectrophotometric data are available. In the table, we do not present the results for the He and H8 lines, because in the case of low-dispersion spectroscopy these are generally blended with, respectively, [Ne III] and He I lines of comparable intensity.

The observed Balmer line ratios are presented in the subsequent columns of Table 5 for the spectra corresponding to slit positions 1a1 and 3a1 and for two different cases: first, we have the ratios obtained when the Savage & Mathis (1979) extinction curve is applied (the column labeled "SM"); second, we have the same ratios for the case in which the procedure based on the general extinction curve by Cardelli et al. (1989) is used (the columns labeled "CCM"; see § 3.1). Two cases are considered: in the first, we adopt the CCM extinction curve with $R_V = 3.1$ (which should, in principle, be equivalent to the Savage & Mathis curve); in the second one, we adopt the composite procedure described in § 3.1, correcting the spectra first by the foreground extinction with $E_{B-V_f} = 0.35$ and $R_V = 3.1$ and later by the remaining extinction with $R_V = 5.5$.

TABLE 5

BALMER LINE RATIOS

LINES	$T_e = 10^4$ K, $N_e = 10^3$ cm^{-3} CASE B	SLIT POSITION 1A1 SM $R_V = 3.1$	CCM $R_V = 3.1$	CCM Composite
Hα/Hβ	2.863	2.895	2.891	2.892
Hγ/Hβ	0.468	0.467	0.505	0.499
Hδ/Hβ	0.259	0.254	0.284	0.280
H9/Hβ	0.073	0.075	0.086	0.084
H10/Hβ.....	0.053	0.043	0.050	0.049
LINES	$T_e = 10^4$ K, $N_e = 10^3$ cm^{-3} CASE A	SLIT POSITION 1A1 SM $R_V = 3.1$	CCM $R_V = 3.1$	CCM $E_{B-V_f} = 0.35$
Hα/Hβ	2.808	2.843	2.829	2.836
Hγ/Hβ	0.474	0.486	0.593	0.543
Hδ/Hβ	0.264	0.253	0.340	0.298
H9/Hβ	0.076	0.071	0.103	0.087
H10/Hβ.....	0.055	0.045	0.065	0.054
LINES	$T_e = 10^4$ K, $N_e = 10^2$ cm^{-3} CASE B	SLIT POSITION 3A1 SM $R_V = 3.1$	CCM $R_V = 3.1$	CCM $E_{B-V_f} = 0.35$
Hα/Hβ	2.857	2.879	2.891	2.892
Hγ/Hβ	0.469	0.484	0.588	0.530
Hδ/Hβ	0.259	0.252	0.336	0.288
H9/Hβ	0.073	0.071	0.102	0.083
H10/Hβ.....	0.053	0.044	0.064	0.052
LINES	$T_e = 10^4$ K, $N_e = 10^2$ cm^{-3} CASE A	SLIT POSITION 3A1 SM $R_V = 3.1$	CCM $R_V = 3.1$	CCM $E_{B-V_f} = 0.35$
Hα/Hβ	2.821	2.865	2.860	2.861
Hγ/Hβ	0.473	0.469	0.508	0.502
Hδ/Hβ	0.264	0.255	0.287	0.282
H9/Hβ	0.076	0.075	0.087	0.085
H10/Hβ.....	0.055	0.043	0.050	0.049

For the spectra at slit positions 1a1 and 3a1, comparison of the observed ratios with the theoretical ones indicates the following:

1. The data do not have enough accuracy to test for case A and case B of recombination theory. The different schemes for correcting extinction allow for much larger variations between line ratios than those arising from different optical depths to Lyman lines.
2. On the one hand, if we adopt the SM extinction curve, all the Balmer line ratios are consistent with the theoretical predictions. The ratio Hγ/Hβ would slightly favor case A predictions, while case B seems to be favored by the ratios H9/Hβ and H10/Hβ. At any rate, the differences between observed and theoretical line ratios are too small to allow us to choose between these two alternatives.
3. On the other hand, if we adopt the CCM extinction curve with $R_V = 3.1$, observed line ratios provide significant discrepancy with the theoretical predictions, for both case A and case B assumptions. The discrepancy is in the sense that higher-order Balmer lines become too strong (notice, e.g., the Hγ, Hδ, H9, and H10 line intensities). The Hα/Hβ ratio remains virtually unchanged because it is used to derive the amount of extinction in any case.
4. The above situation still holds true if we adopt the two-component extinction correction, with $R_V = 3.1$ for the foreground extinction of $E_{B-V_f} = 0.35$, and $R_V = 5.5$ for the remaining extinction.

The above remarks apply also to the remaining extractions. We conclude that the SM procedure is more suitable in the present observed complexes than the CCM procedure. We remark that the difference between the corrections furnished by the two extinction curves, for the case $R_V = 3.1$, is very small as long as we have low values of E_{B-V}. In the case of the H II regions that we observed, however, the extinction is relatively high, and using one or another approach produces sizeable differences in the final results.

Although observations are not accurate enough to distinguish between case A and case B, we note that the electron density in the region sampled by the slit position 1a1 is very high, so that therein case B would certainly be a better assumption than case A. With respect to the role played by dust—which can also lead to deviations from the case B line emissivities—its effect causes line ratios intermediate between case A and case B, so that not much can be inferred from the present data.

Finally, for the abundance analysis that will be performed later in this paper, we will assume the Savage & Mathis extinction curve, and case B conditions, as a consequence of the conclusions above.

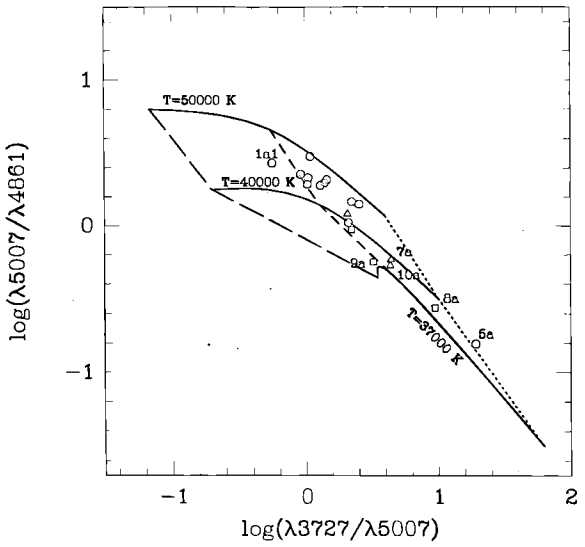

FIG. 5*a*

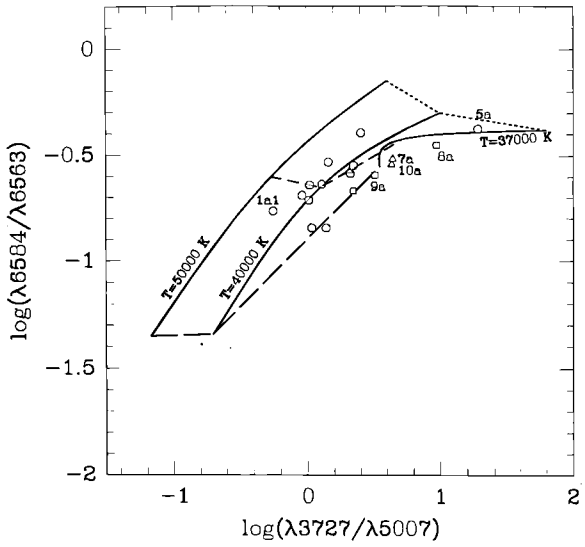

FIG. 5*b*

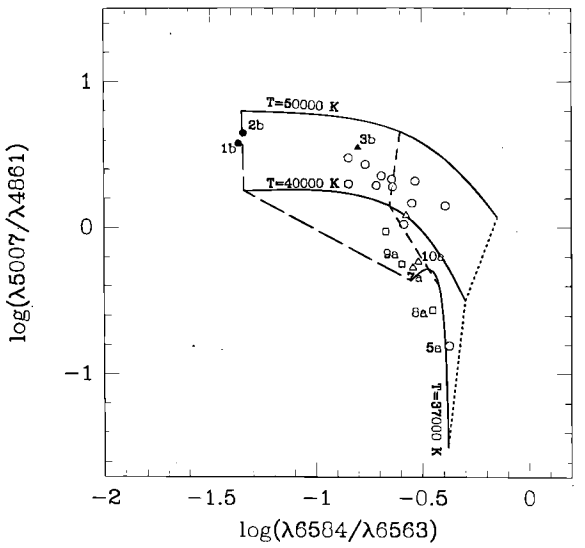

FIG. 5*c*

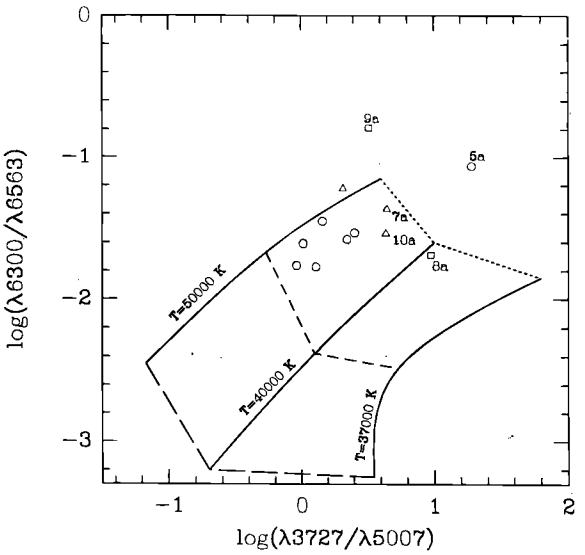

FIG. 5*d*

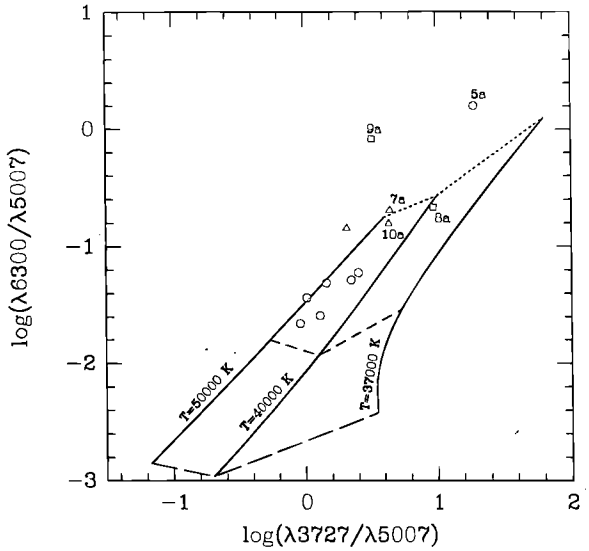

FIG. 5*e*

FIG. 5.—Line ratios in diagnostic diagrams, for knots (*circles*), diffuse regions (*triangles*), and filaments (*squares*). Empty symbols are for Gum 38a spectra, filled ones for Gum 38b spectra. The lines are the set of Evans & Dopita's (1985) models for T_i = 37,000, 40,000, and 50,000 K and for log $U = -2.5$ (*dotted line*), -1.5 (*short-dashed line*), and -0.5 (*long-dashed line*).

3.3. *Diagnostic Diagrams*

Figure 5 shows the position of the spectra in several diagnostic diagrams involving the main H I, [O II], [O III], [N II], and [O I] lines. These diagrams can be used to separate nebulae with different ionization mechanisms (Baldwin, Phillips, & Terlevich 1981). A subset of Evans & Dopita's (1985) models shows that the sequence followed by normal H II regions (more clearly seen in Figs. 5*a*, 5*b*, and 5*c*) can be interpreted as one of excitation conditions: from left to right in the diagrams, we have decreasing temperature of the ionizing star T_i and decreasing mean ionization parameter $U = \bar{Q}(\mathrm{H})/c$, with $Q(\mathrm{H}) = L_C/(4\pi r^2 N)$ (see Evans & Dopita 1985).

We emphasize that Evans & Dopita's models refer to integrated H II regions, whereas our spectra are for lines of sight through a spatially resolved H II region. Nevertheless, the comparison provides interesting conclusions on the ionization and excitation mechanisms in Gum 38a and 38b. In Figures 5*a*, 5*b*, and 5*c*, most of the observed points are within the boundaries defined by the models of normal H II regions. Also, there is a gradient in excitation conditions within the Gum 38a region: the central knots of the nebula are more excited than the neighboring diffuse regions and filaments. In the diagrams, the knots occupy the locus of nebulae photoionized by stars with T_i between 40,000 and 50,000 K. Diffuse regions and filaments are characterized by a low ionization parameter, closer to $\log U = -2.5$, and possibly by lower temperatures T_i.

Figures 5*d* and 5*e*, which involve the [O I] λ6300 line, appear to separate more clearly the effects of changing T_i and the ionization parameter. They also indicate that T_i is in the range 40,000–50,000 K for most of the diffuse regions and filaments. It should be noted that, in general, H II regions, when observed integratedly, or at their brightest parts, present values of both $\log(\lambda 6300/\lambda 6563)$ and $\log(\lambda 6300/\lambda 5007)$ lower than -2. In present extractions corresponding to the brightest knots (NGC 3581 and NGC 3586), [O I] λ6300 is below the detectability limit, and consequently the diagnostic diagrams Figures 5*d* and 5*e* are not populated in their bottom. The fainter, more external knots and diffuse regions occupy the upper part of the diagrams, corresponding to low ionization parameter values.

There are two noteworthy cases that deviate considerably from the models, suggesting very low ionization parameters. One is the knot at slit position 5a (NGC 3576), which is quite compact ($\sim$1 pc in diameter). In order to explain the low ionization parameter, we should invoke an extremely high nebular density, assuming that the ionizing star is inside the nebula. Nevertheless, the ratio of the [S II] (Table 4) indicates normal densities. A more reasonable interpretation is that the ionizing star is outside the nebula.

The second case is the extraction at slit position 9a, which corresponds to the sharp semicircular filament seen to the north of Gum 38a (Fig. 1). In Figures 5*a*, 5*b*, and 5*c*, its locus is similar to those of apertures 7a and 10a. However, in Figures 5*d* and 5*e*, it is located away from them, with an unusually strong [O I] λ6300. Notice that we are dealing with a well-defined bright filament, whereas at slit positions 7a and 10a we have faint diffuse regions. The strong [O I] could be understood in terms of photoionization only if its line of sight is along a partially ionized H II region edge.

The slit position 8a samples the southern part of the long arc in Gum 38a (Fig. 1). This nebula is apparently not associated with embedded OB stars, and its ionizing sources might be the OB stars at the center of the complex, at projected distances of $\sim$5 pc. In this case, the ionizing parameter is expected to be low, as confirmed in Figures 5*d* and 5*e*.

The comparison between line ratios observed in particular lines of sight with those predicted by integrated models (Figs. 5*a*, 5*b*, and 5*c*) suggests that for central regions the ionizing star temperature is $T_i \simeq 40{,}000$–$50{,}000$ K, whereas for outer diffuse zones of the same complexes, $T_i < 40{,}000$ K. This emphasizes the need of computing line-of-sight models to study the ionization structure. Nevertheless, the temperatures above indicate that the B0 stars HD 97499 and CPD $-60°2641$ do not provide enough ionizing photons to explain the inferred ionization structure. Indeed, Smith, Biermann, & Mezger (1978) estimated that 26.1×10^{49} Lyman continuum photons per second were necessary to produce the observed radio fluxes in Gum 38a. This corresponds roughly to four O5 stars. As a matter of fact, Gum 38a hosts a group of IR sources (Frogel & Persson 1974), which might be strongly reddened O stars in dust cocoons. A small leaking fraction of their ultraviolet flux could produce the observed ionization structure.

For Gum 38b, there is no doubt that the central star cluster NGC 3603 provides the bulk of ionizing photons. The decrease of the ionization parameter in the outer region (3b) relative to the inner ones (1b and 2b) (Fig. 5*c*) can be easily understood as the result of dilution of the cluster radiation field.

3.4. *Electron Temperatures and Densities*

Electron temperature estimates are available for two extractions in Gum 38a, by means of the [O III] $\lambda\lambda$4959, 5007/λ4363 ratio, and for 3 by [N II] $\lambda\lambda$6548, 6583/λ5755. Electron densities were derived from the [S II] λ6717/λ6732 line ratio. We used De Robertis, Dufour, & Hunt's (1987) code, based on the five-level atom approximation, to derive $T_{[\mathrm{O\,III}]}$, $T_{[\mathrm{N\,II}]}$, and N_e. The derived values are presented in Table 4. In regions of Gum 38a where the temperature was not available, we assumed $T_{[\mathrm{O\,III}]} = 9000$ K, whereas for those of Gum 38b we adopted $T_{[\mathrm{O\,III}]} = 10{,}000$ K. These temperatures were used for the calculation of the Balmer decrements (§ 3.1).

The calculations indicate that knots have typical densities in the range 500–1000 cm^{-3}, whereas diffuse and filamentary regions have densities in the range 100–300 cm^{-3}.

In the present spectra of Gum 38b the line [O III] λ4363 is not detectable, so we used the data presented by MTT89 to estimate $T_{[\mathrm{O\,III}]} \simeq 9800$ K and $N_e \simeq 5200$ cm^{-3} for the region corresponding to slit position 1b. The resulting density difference as compared with our values (see Table 4) probably arises from their sampling more central and denser parts of the nebula.

3.5. *Chemical Abundances*

Chemical abundances were derived only for the spectra at slit positions 1a1, 3a1, and 1b, for which we have good temperature determinations. Following the formalism developed by Peimbert & Costero (1969), the H II region emission along a line of sight can be considered as originating from a high-ionization zone, which contains most of the He^+, O^{++}, S^{++}, and Ne^{++}, and a low-ionization one containing O^+, S^+, N^+, and some neutral atoms as O^0. In fact, the O^0 emission arises in the partially ionized layer at the

TABLE 6

IONIC AND ELEMENTAL ABUNDANCES FOR REGIONS AT SLIT POSITIONS 1A1, 3A1, AND 1B, COMPARED WITH THOSE OF THE ORION NEBULA

Ion/Element	1a1	3a1	1b	Orion	$\Delta_{(t^2=0.02)}$	$\Delta_{(t^2=0.04)}$
$He^+/H^+(\lambda 4472)$	0.0939 ± 0.0042	$0.1020^{+0.0085}_{-0.0120}$	...	0.0952 ± 0.0083	...	...
$He^+/H^+(\lambda 5876)$	0.0967 ± 0.0008	$0.0830^{+0.0015}_{-0.0021}$	~0.115	0.1040 ± 0.0015	...	...
$He^+/H^+(\lambda 6678)$	0.0917 ± 0.0034	$0.0767^{+0.0054}_{-0.0075}$	~0.096	0.0958 ± 0.0063	...	...
He^+/H^+(mean).....	0.0955 ± 0.0015	$0.0864^{+0.0029}_{-0.0041}$	~0.106	0.0981 ± 0.0028	−0.0012	−0.0024
$12 + \log(N^+/H^+)$.....	7.20 ± 0.08	$7.45^{+0.29}_{-0.18}$	6.83	7.15 ± 0.05	0.08	0.17
$12 + \log(O^0/H^+)$	...	$7.49^{+0.39}_{-0.24}$	...	6.96 ± 0.05	0.12	0.25
$12 + \log(O^+/H^+)$.....	8.18 ± 0.14	$8.55^{+0.49}_{-0.29}$	7.64	8.24 ± 0.11	0.08	0.16
$12 + \log(O^{++}/H^+)$.....	8.30 ± 0.08	$8.08^{+0.26}_{-0.15}$	8.27	8.25 ± 0.05	0.12	0.25
$12 + \log(Ne^{++}/H^+)$.....	7.35 ± 0.09	$7.16^{+0.31}_{-0.20}$	7.18	7.32 ± 0.06	0.12	0.25
$12 + \log(S^+/H^+)$	5.84 ± 0.08	$6.16^{+0.28}_{-0.17}$	5.04	5.71 ± 0.12	0.08	0.16
$12 + \log(S^{++}/H^+)$	6.80 ± 0.10	$6.82^{+0.33}_{-0.21}$	...	6.94 ± 0.05	0.17	0.36
$12 + \log(Ar^{++}/H^+)$	6.21 ± 0.06	$5.98^{+0.18}_{-0.11}$	...	6.29 ± 0.05	0.09	0.20
He/H	0.1017 ± 0.0014	$0.0993^{+0.0030}_{-0.0042}$	...	0.0931 ± 0.0027	~ −0.035	~ −0.0070
$12 + \log$(N/H)	7.56 ± 0.05	$7.58^{+0.24}_{-0.13}$	7.55	7.46 ± 0.04	0.10	0.21
$12 + \log$(O/H)	$8.55^{+0.12}_{-0.09}$	$8.67^{+0.44}_{-0.25}$	8.36	8.55 ± 0.06	0.10	0.21
$12 + \log$(S/H).....	7.49 ± 0.07	$7.03^{+0.26}_{-0.16}$	...	7.27 ± 0.07	0.17	0.38
$12 + \log$(Ne/H).....	7.40 ± 0.12	$7.75^{+0.49}_{-0.28}$	7.27	7.63 ± 0.07	0.10	0.21

NOTE.—The last two columns present the abundance increase for assumed temperature fluctuations of $t^2 = 0.02$ and $t^2 = 0.04$.

edge of the Strömgren sphere, where H^+ coexists with H^0. The electronic temperatures $T_h = T_{[O\ III]}$ and $T_l = T_{[N\ II]}$ were taken as representative, respectively, of the high- and low-ionization zones.

He^+ abundances were calculated from the $\lambda\lambda$4471, 5876, and 6678 lines using the effective emission coefficients from Brocklehurst (1972). The density-dependent correction for collisional excitation from the metastable level $2\ ^3S$ of He I was made according to Clegg (1987). The derived abundances (Table 6) from these lines are in reasonable agreement. A weighted mean abundance is also presented in the table.

To calculate the abundances of metallic ions from the forbidden lines, we used the five-level atom approximation according to De Robertis et al.'s (1987) code. We remark that several of the atomic parameters have been updated in the version of the code kindly provided by Dr. De Robertis in 1996. For each ion X^{+n} for which a forbidden line $\lambda(X^{+n})$ was available, the abundance relative to H^+ was given by

$$\frac{N(X^{+n})}{N(H^+)} = \frac{F_{\lambda(X^{+n})}}{F_{H\beta}} \frac{\epsilon_{H\beta}}{\epsilon_{\lambda(X^{+n})}}, \quad (5)$$

where $\epsilon_{H\beta}$ and $\epsilon_{\lambda(X^{+n})}$ are, respectively, the line emissivity at $H\beta$ (Storey & Hummer 1995) and the line emissivity at the forbidden line given by De Robertis et al.'s code. The following lines were used: [O I] λ6300 for O^0, [O II] λ3727 for O^+, [O III] $\lambda\lambda$4959, 5007 for O^{++}, [N II] $\lambda\lambda$6548, 6583 for N^+, [Ne III] λ3869 for Ne^{++}, [S II] $\lambda\lambda$6717, 6731 for S^+, [S III] λ6312 for S^{++}, and [Ar III] λ7136 for Ar^{++}. The derived ionic abundances are listed in Table 6.

In order to convert the ionic abundances to total elemental ones, we used the ionization correction factors (ICFs) scheme suggested by Peimbert & Costero (1969), namely,

$$\frac{O}{H} = \frac{O^+ + O^{++}}{H^+}, \quad \frac{N}{H} = \frac{O}{O^+}\frac{N^+}{H^+}, \quad \frac{Ne}{H} = \frac{O}{O^{++}}\frac{Ne^{++}}{H^+},$$

$$\frac{S}{H} = \frac{O}{O^+}\frac{S^+ + S^{++}}{H^+}, \quad \frac{He}{H} = \frac{S}{S - S^+}\frac{He^+}{H^+}, \quad (6)$$

which are based on simple considerations about the relative sizes of differently ionized regions. The above ICFs were compared with those computed from model nebulae by Mathis (1985), and the differences were, in all cases, lower than 30%. Table 6 presents the derived abundances. In the case of argon, we show that of Ar^{++}, since the corresponding ICF is uncertain (Mathis 1985); however, from our O^+/O^{++} and S^+/S^{++} ratios, we estimate that Ar^{++}/Ar should be ~0.6.

The last two columns of Table 6 present the increase in abundances when we assume the existence of temperature fluctuations along the line of sight, according to Peimbert & Costero's (1969) formalism. Two values of the mean square temperature variation t^2 are considered. We recall that t^2 values of ~0.35–0.55 have been considered appropriate for the Orion Nebula (Peimbert & Torres-Peimbert 1977; Walter, Dufour, & Hester 1992). Basically, the metallic element abundances increase by 0.1 dex and 0.2 dex, respectively, for $t^2 = 0.02$ and 0.04, except in the case of sulphur, for which the effect is somewhat stronger.

The abundance determinations that we have performed are somewhat dependent on the adopted assumptions. For instance, if we adopted case A of recombination theory, the emissivities at $H\beta$ would be ~1.5 times lower (cf. Storey & Hummer 1995), lowering the metallic abundances by the same factor (see eq. [5]). The same effect could be caused by the absorption of Lyman photons by dust. Also, Peimbert & Costero's ICF scheme is an approximate description of real ionized nebulae. These uncertainties should be kept in mind for the analysis of the chemical abundances that we presented for Gum 38a and 38b. It is worth comparing these results with those of the Orion Nebula, using the same methods. This nearby H II region is largely considered as a reference object for abundance determinations, and detailed studies of their structure and abundances have been published (see, e.g., Baldwin et al. 1991; Osterbrock, Tran, & Veilleux 1992).

We applied the same methods described above to the spectra of the Orion Nebula numbered 1–5 in Baldwin et

al.'s (1991) work. These spectra cover a region of the Orion Nebula very close (40′–70′) to the central θ^1 Ori C ionizing star. Each spectrum has been analyzed separately, and the fifth column of Table 6 presents the mean of the values derived for the ionic abundances. The abundances of each ionic species of oxygen are similar to those derived for the slit position 1a1 (Gum 38a). Consequently, the central part of the Gum 38a complex presents an ionization structure similar to that of the central part of Orion.

We present in the fifth column of Table 6 the resulting mean elemental abundances for Orion. As a check, our abundance determinations were compared with those derived by other authors. Our value of He/H = 0.093 is intermediate between those of Osterbrock et al. (1992) and Baldwin et al. (1991): respectively, 0.101 and 0.088. The same occurs for oxygen (8.55 against 8.49 and 8.58). For nitrogen, our value is somewhat below both (7.46 against 7.72 and 7.93); for sulphur, our value is slightly above (7.27 against 6.97 and 7.12), whereas for neon our value resembles that of the former authors (7.63 against 7.60 and 8.60). The agreement is good considering the uncertainties involved, such as different sources of data and/or methods. The important point is that in the subsequent comparison of Gum 38a and Orion the employed methods were the same.

The N, O, and Ne abundances are similar in Gum 38a and Orion, but S in Orion is nearly twice that in Gum 38a, while that of He is $\sim$5% lower. These differences, however, might reflect an overestimation of the temperature in the S^{++} zone for the Gum 38a regions, which in turn would decrease He/H via the ICF (eq. [6]). We recall that S^{++} abundances in Gum 38a were calculated by means of the weak [S III] λ6312 line, which is more dependent on temperature than the [S III] λ9532 line used in Orion. Thus, the He and S abundance values should be taken with caution. The oxygen abundance, on the contrary, is expected to be the most accurate because we see strong lines of the two major ionization stages of this element. We conclude that the O abundances for Gum 38a and Orion are similar to within a $\sim$0.1 dex error. Similar O abundances are found for Gum 38b (Table 6), but in this case the error is probably larger.

The similarity of abundances in Gum 38a, Gum 38b, and the Orion Nebula, especially for the well-determined oxygen values, is consistent with these regions being at similar Galactocentric radii (respectively, 7.1, 8.3, and 7.9 kpc, adopting $R_{GC\odot} = 7.5$ kpc). This is expected since no significant abundance differences arise from the Galactic gradient, which is probably lower than 0.1 dex kpc^{-1} (e.g., Shaver et al. 1983).

4. CONCLUDING REMARKS

The present long-slit spectrophotometry in the H II region complexes Gum 38a and Gum 38b allowed us to derive information on their reddening distribution, ionization structure, and chemical content. The main conclusions are as follows:

1. We find upper limits to the foreground reddening of $E_{B-V_f} = 0.35$ for Gum 38a and $E_{B-V_f} = 1.65$ for Gum 38b. In the central knots of Gum 38a, the typical internal reddening is $E_{B-V_i} \simeq 0.35$. The spatial distribution of reddenings confirms that Gum 38b is farther away from us than Gum 38a. We found that for the present complexes, Savage & Mathis's (1979) extinction curve provides Balmer line ratios that are consistent with the theoretical predictions, whereas some significant deviations occur when the extinction curve of Cardelli et al. (1989) is used.

2. In Gum 38a, the B0 stars HD 97499 and CPD $-60°2641$ do not appear to be hot enough to explain the observed ionization structure: a leak of ultraviolet flux from dust-absorbed O stars can account for it. This is corroborated by the presence of infrared sources inside the knot NGC 3581 and observed integrated radio flux. Some external filaments and diffuse regions appear to be at least in part ionized by the outlying O5 star HD 97484.The outlying knot NGC 3576 presents a too low ionizing parameter, which suggests that its ionizing radiation might come from outside the knot, possibly stars in the central knot NGC 3581. The extended diffuse emission and filaments in the vicinity of the knots are also probably ionized by the stars in the central knots, as denoted by the lower ionization parameters, because of the radiation field dilution.

3. A bright filament in the northern parts of Gum 38a (at slit position 9a) presents unusually strong [O I] $\lambda\lambda$6300, 6364 lines. A possible explanation is that the observed line of sight samples the partially ionized edge of an H II region (§ 3.3). These oxygen lines could be enhanced if shock ionization were present. Nevertheless, the [S II] $\lambda\lambda$6717, 6731 lines do not appear to be significantly enhanced in the filament, as is the case of model and observed shocked regions (e.g., Osterbrock 1988; Sutherland, Bicknell, & Dopita 1993). Slit position 9a samples the brightest part of a semicircular structure containing the O5 star HD 97484 (Fig. 1). The filament is possibly part of a bubble surrounding this star, which is located at a projected distance of approximately 3.4 kpc from the filament.

4. For Gum 38b, the central cluster NGC 3603 provides the bulk of ionizing photons, and the diffuse emission regions in the northern parts of the nebula differ from the central regions only by having a lower ionization parameter, as a result of dilution of the cluster's radiation field.

5. The O, N, and Ne chemical abundances in Gum 38a and Gum 38b are comparable to those of the Orion Nebula. The three objects are located at similar Galactocentric distances and appear to share the chemical properties of solar-vicinity H II regions.

It is worth commenting the results above in the frame of the environment where the complexes are located. Johnston et al. (1992), in a survey for pulsars in the southern hemisphere, suggested the association of the newly found pulsar PSR 1112−60 to the RCW 57 complex. Out of 100 pulsars detected in the survey, it was the only one apparently related to a known H II region. Figure 1, however, shows that PSR 1112−60 is located outside of the emission region. In fact, the background sky spectra taken nearby the pulsar's location provide an upper limit for the Hβ flux of only 2.8×10^{-6} ergs s^{-1} cm^{-1} sr^{-1} (a factor of $\sim$200 times smaller than in the knot NGC 3581 [slit position 1a1], and $\sim$5 smaller than in the faintest diffuse or filamentary regions). Also, the radio maps of Shaver & Goss (1970) do not show a radio continuum in the pulsar region. The pulsar in the line of sight does not cross a region with a significant density of ionized gas; Johnston et al.'s large dispersion measure (DM = 680 cm^{-3} pc) would, rather, imply that it is located in the background of Gum 38a and 38b. Indeed, at the distances of Gum 38a and Gum 38b, the pulsar should present DM = 140 and 267 cm^{-3} pc, respec-

tively, taking Taylor & Cordes's (1993) model for the distribution of free electrons in the Galaxy. Therefore, we can confidently conclude that this pulsar is not associated to the H II regions observed in its vicinity.

Gum 38a might be related to the Car OB2 association (see Fig. 1 of Garcia 1993; therein Gum 38a is designated as NGC 3576). The distance of Car OB2 found by Garcia is similar to that of Gum 38a. We suggest that Gum 38a is part of a long arc consisting of OB stars, H II regions, and young star clusters; Clariá (1976) indicated that the objects NGC 3572, Hogg 10, 11, and 12, Trumpler 18, and NGC 3590 were related to Car OB2. We speculate that Gum 38a would be the youngest component of this larger OB structure, possibly the result of an interaction between the shell that originated the Car OB2 complex and the molecular/dust cloud to the south of Gum 38a.

The morphology of Gum 38a makes it an interesting object for further studies on its ionization structure and kinematics. In particular, since it is similar to Orion in terms of morphology, and by the fact that it is located at the edge of a molecular cloud, it would be worth testing the champagne flow scenario by means of high-dispersion spectroscopic observations in order to obtain its velocity field.

We are grateful to the CTIO staff for hospitality and assistance during the observations. We thank Dr. De Robertis for sending us his computer code and an anonymous referee for interesting remarks. We acknowledge financial support from the Brazilian Institutions CNPq and FINEP.

REFERENCES

Baldwin, J. A., Ferland, G. J., Martin, P. G., Corbin, M. R., Cota, S. A., Peterson, B. M., & Slettebak, A. 1991, ApJ, 374, 580
Baldwin, J. A., Phillips, M. M., & Terlevich, R. 1981, PASP, 93, 5
Balick, B., Boeshaar, G. O., & Gull, T. R. 1980, ApJ, 242, 584
Block, D. 1990, Messenger, 60, 32
Brocklehurst, M. 1972, MNRAS, 157, 211
Cardelli, J. A., Clayton, G. C., & Mathis, J. S. 1989, ApJ, 345, 245
Clariá, J. J. 1976, AJ, 81, 155
Clegg, R. E. S. 1987, MNRAS, 229, 31P
Crampton, D., & Georgelin, Y. M. 1975, A&A, 40, 317
De Robertis, M. M., Dufour, R. J., & Hunt, R. W. 1987, JRASC, 81, 195
Evans, I. N., & Dopita, M. A. 1985, ApJS, 58, 125
Frogel, J. A., & Persson, S. E. 1974, ApJ, 192, 351
Garcia, B. 1993, ApJS, 87, 197
Ghosh, S. K., Iyengar, K. V. K., Rengarajan, T. N., Tandon, S. N., Verma, R. P., & Daniel, R. R. 1989, ApJS, 69, 233
Gillespie, A. R., Huggins, P. J., Sollner, T. C. L. G., Phillips, T. G., Gardner, F. F., & Knowles, S. H. 1977, A&A, 60, 221
Goss, W. M., & Radhakrishnan, V. 1969, Astrophys. Lett., 4, 199
Goss, W. M., Radhakrishnan, V., Brooks, J. W., & Murray, J. D. 1972, ApJS, 24, 123
Gum, C. S. 1955, MmRAS, 67, 155
Hummer, D. G., & Storey, P. J. 1992, MNRAS, 254, 277
Humphreys, R. M. 1978, ApJS, 38, 309
Johnston, S., Lyne, A. G., Manchester, R. N., Kniffen, D. A., D'Amico, N., Lim, J., & Ashworth, M. 1992, MNRAS, 255, 401
Kuiper, T. B. H., Whiteoak, J. B., Fowler, J. W., & Rice, W. 1987, MNRAS, 227, 1013
Lacy, J. H., Beck, S. C., & Geballe, T. R. 1982, ApJ, 255, 510
Mathis, J. S. 1985, ApJ, 291, 247
Mathis, J. S., & Wallenhorst, S. G. 1981, ApJ, 244, 483
Melnick, J., Tapia, M., & Terlevich, R. 1989, A&A, 213, 89 (MTT89)
Moneti, A. 1992, A&A, 259, 627
Osterbrock, D. E. 1988, Astrophysics of Gaseous Nebulae and Active Galactic Nuclei (Mill Valley: University Science)
Osterbrock, D. E., Tran, H. D., & Veilleux, S. 1992, ApJ, 389, 305
Peimbert, M., & Costero, R. 1969, Bol. Obs. Tonantzintla Tacubaya, 5, 3
Peimbert, M., & Torres-Peimbert, S. 1977, MNRAS, 179, 217
Retallack, D. S., & Goss, W. M. 1980, MNRAS, 193, 261
Rodgers, A. W., Campbell, C. T., & Whiteoak, J. B. 1960, MNRAS, 121, 103
Santos, J. F. C., Jr., & Bica, E. 1993, MNRAS, 260, 915
Savage, B. D., & Mathis, J. S. 1979, ARA&A, 6, 215
Shaver, P. A., & Goss, W. M. 1970, Australian J. Phys. Astrophys. Suppl., 14, 133
Shaver, P. A., McGee, R. X., Newton, L. M., Danks, A. C., & Pottasch, S. R. 1983, MNRAS, 204, 53
Smith, L. F., Biermann, P., & Mezger, P. G. 1978, A&A, 66, 65
Stone, R. P. S., & Baldwin, J. A. 1983, MNRAS, 193, 219
Storey, P. J., & Hummer, D. G. 1995, MNRAS, 272, 41
Sutherland, R. S., Bicknell, G. V., & Dopita, M. A. 1993, ApJ, 414, 510
Taylor, J. H., & Cordes, J. M. 1993, ApJ, 411, 674
Tenorio-Tagle, G. 1979, A&A, 71, 59
Walter, D. K., Dufour, R. J., & Hester, J. J. 1992, ApJ, 397, 196